

Putting eagle rays on the map by coupling aerial video-surveys and deep learning

Highlights

- Efficient techniques are needed to monitor vulnerable elasmobranchs in space and time.
- Deep learning applied to images is a powerful tool for automated wildlife monitoring.
- Our deep learning model successfully detected 92% of eagle rays on images.
- This study is a step forward for ray monitoring in coral reef ecosystems.

Keywords

Automated species detection, convolutional neural networks, coral reefs, elasmobranchs, New-Caledonia

Abstract

Reliable and efficient techniques are urgently needed to monitor elasmobranch populations that face increasing threats worldwide. Aerial video-surveys provide precise and verifiable observations for the rapid assessment of species distribution and abundance in coral reefs, but the manual processing of videos is a major bottleneck for timely conservation applications. In this study, we applied deep learning for the automated detection and mapping of vulnerable eagle rays from aerial videos. A light aircraft dedicated to touristic flights allowed us to collect 42 hours of aerial video footage over a shallow coral lagoon in New Caledonia (Southwest Pacific). We extracted the videos at a rate of one image per second before annotating them, yielding 314 images with eagle rays. We then trained a convolutional neural network with 80% of the eagle ray images and evaluated its accuracy on the remaining 20% (independent data sets). Our deep learning model detected 92% of the annotated eagle rays in a diversity of habitats and acquisition conditions across the studied coral lagoon. Our study offers a potential breakthrough for the monitoring of ray populations in coral reef ecosystems by providing a fast and accurate alternative to the manual processing of aerial videos. Our deep learning approach can be extended to the detection of other elasmobranchs and applied to systematic aerial surveys to not only detect individuals but also estimate species density in coral reef habitats.

29 **1. Introduction**

30 Elasmobranchs, a subclass of cartilaginous fishes composed of sharks, rays, skates and sawfish,
31 are among the most endangered animal taxa in the oceans (Dulvy et al. 2021). These species are
32 intrinsically sensitive to human activities due to their slow growth rate and limited reproduction
33 capacity, preventing them from quickly recovering from overexploitation (Pacoureaux et al., 2021).
34 Elasmobranchs are primarily threatened by targeted fisheries and incidental catches, although
35 habitat degradation is a growing threat for coastal species (Dulvy et al. 2021; Yan et al. 2021).
36 Within the 1,199 species of elasmobranchs assessed by the IUCN in 2021, 10.4% were listed as
37 near-threatened, 15% as vulnerable, 10.1% as endangered (compared to 4.1% in 2010), 7.5% as
38 critically endangered, and 12.9% as data deficient (Dulvy et al. 2021). Rays are even more
39 threatened than sharks with 36% of all species threatened compared to 31.2% (Dulvy et al. 2021).
40 Currently, the limited knowledge and monitoring of elasmobranch abundance and distribution is a
41 major impediment to the implementation of targeted conservation measures (Jabado et al., 2018).
42 To fill these knowledge gaps, new techniques are urgently needed to efficiently and rapidly monitor
43 threatened elasmobranchs in space and time in order to identify their key habitats and provide
44 abundance estimates at the basis of IUCN assessments.

45 Video-surveys from drones or light aircraft are increasingly used to assess the distribution,
46 behavior and abundance of marine megafauna (Hodgson, Kelly, and Peel 2013; Kelaher et al.
47 2020; Schofield et al. 2017). Such digital surveys are particularly suited to study sharks and rays in
48 coral lagoons where clear and shallow waters facilitate their detection (Kiszka et al., 2016; Rieucoux
49 et al., 2018). Video-surveys offer important advantages over traditional observer-based surveys by
50 generating precise and verifiable observations that are free from observer fatigue and subjectivity
51 (Colefax, Butcher, and Kelaher 2018; Kelaher et al. 2019). However, manual video analysis is a
52 major bottleneck for timely conservation applications, as visualizing hours of footage is both
53 extremely time-consuming and error-prone (Ditria, 2020; Norouzzadeh et al., 2018; Villon et al.,
54 2018). Deep learning algorithms offer great promises to overcome this limitation by allowing the
55 automated identification and detection of species on images (Christin, Hervet, and Lecomte 2019;
56 Norouzzadeh et al. 2018; Torney et al. 2019; Eikelboom et al. 2019). Such models have been
57 successfully applied for the detection of sea turtles (Dujon et al., 2021; Gray et al., 2018), dugongs
58 (Mannocci et al., 2021), pinnipeds (Dujon et al., 2021; Padubidri et al., 2021) and whales (Gray et
59 al. 2019; Guirado et al. 2019). Although there are a few applications for elasmobranchs, these are
60 generally dedicated to monitoring shark risks (Gorkin et al., 2020) rather than conservation
61 objectives requiring abundance and distribution estimates. Accurate deep learning models would
62 drastically increase the efficiency of aerial monitoring for these threatened species.

63 In this study, we combined aerial video-surveys and deep learning to detect eagle rays and map
64 their distribution throughout a lagoon in New Caledonia, Southwest Pacific. New Caledonia hosts
65 exceptional coral reefs and lagoons, which form one of the three most extensive reef systems in
66 the world (Ceccarelli et al., 2013). Eagle rays are conspicuous rays of the Myliobatidae family that
67 are easily spotted from the surface owing to their relatively large size and characteristic diamond
68 shape (Last, White, and Pogonoski 2010), making them good candidates for automated detection
69 on aerial images. Two species of Myliobatidae are present in New Caledonia, the spotted eagle
70 ray, *Aetobatus narinari* which is common, and the rarer mottled eagle ray, *Aetomylaeus maculatus*
71 (Fricke, Kulbicki, and Wantiez 2011). These species have been classified as globally endangered
72 by the IUCN in 2020 (Dulvy et al. 2020; Rigby et al. 2020), stressing the urgent need to monitor the
73 trends of their populations to feed global indicators like the Living Planet Index (Pacoureau et al.,
74 2021). We trained and evaluated a deep learning model to automatically detect eagle rays on
75 aerial images collected from an ultra-light motor plane (ULM). We then mapped their distribution
76 across the studied lagoon. Our study unravels the potential of deep learning applied to aerial
77 surveys for monitoring the distribution of vulnerable elasmobranchs in coral reefs.

78 **2. Material and methods**

79 **2.1. Video data collection**

80 Video-surveys were conducted from an amphibious ULM (AirMax SeaMax) operating touristic
81 flights over the Poé lagoon on the Western coast of New Caledonia (Supplementary Figure A).
82 This lagoon is shallower than 5 m and characterized by shallow reef, seagrass and sandy habitats.
83 The barrier reef includes three deep passes and channels reaching 30 m. Part of the Poé lagoon
84 was declared as a natural reserve (IUCN category IV) in 2006 and is located within the broader
85 South Province Park created in 2009 and the UNESCO World Heritage area established in 2008.
86 A GoPro Hero Black 7 camera was mounted under the right wing of the ULM, pointing downward.
87 The camera was configured to record videos at a rate of 24 frames per second in linear field of
88 view mode at a resolution of 2.7 K (2,704 x 1,520 pixels) with integrated image stabilization. The
89 camera was manually triggered by the pilot before each flight. Telemetry data, including GPS
90 coordinates and altitudes, were also recorded by the GoPro along each flight (at a rate of 8 to 12
91 positions per second). The mean altitude across all flights was 152 m (standard deviation SD= 52
92 m). At this altitude the image covered a mean surface area of 161 m × 287 m corresponding to a
93 ground sampling distance of 11 cm per pixel. In total, over 42 hours of videos representing 36 fly
94 days were collected from September 2019 to January 2020 in good weather conditions.

95 **2.2. Image annotation**

96 Image annotation is a crucial prerequisite before applying deep learning models (Gray et al., 2018;
97 Norouzzadeh et al., 2018; Villon et al., 2020). All videos were first visualized by a team of students
98 who recorded the times at which they spotted eagle rays (and other megafauna species). Videos
99 that contained at least one eagle ray (representing 114 videos from a total of 228 (Table 1)) were
100 then imported into a custom online application (<http://webfish.mbb.univ-montp2.fr/>) (Supplementary
101 Figure B). Next, images were extracted from all videos at a rate of one image per second,
102 representing a compromise between image diversity and annotation time.

103 The annotation procedure consisted in manually drawing rectangle bounding boxes around
104 identified eagle rays and associating labels to these individuals. Only individuals that could be
105 identified without ambiguity as eagle rays, owing to their large size, diamond shape and dark
106 colour, were annotated. Although *Aetomylaeus maculatus* is generally smaller than *Aetobatus*
107 *narinari*, their color patterns are similar (light spots on a dark disc) so they are easily confused *in*
108 *situ*. The presence of a long spine near the tail's base of *A. narinari* can help to differentiate it from
109 *A. maculatus* which has a long but spineless tail (Froese and Pauly 2021). Since we could not
110 distinguish one or the other species on aerial videos we built a generic eagle ray (i.e.,
111 Myliobatidae) detector, although most sightings were likely of *A. narinari* which is much more
112 common in New Caledonia (Fricke et al., 2011). Each annotation yielded a text file containing the
113 coordinates and label of the bounding box, along with the corresponding image in jpeg format
114 (examples of images are provided in Supplementary Figure C).

115 **2.3. Eagle ray detection model**

116 We used a convolutional neural network (CNN), a class of deep learning models that is widely
117 applied for image classification and object detection, i.e., the task of simultaneously localizing and
118 classifying objects on images (LeCun, Bengio, and Hinton 2015). CNNs represent by far the most
119 commonly used category of deep learning models in ecology (Christin, Hervet, and Lecomte 2019).
120 They are formed by stacked groups of convolutional layers and pooling layers that are particularly
121 suited to process image inputs. Convolutional layers extract local combinations of pixels known as
122 'features' from images. In the convolution operation, a filter defined by a set of weights computes
123 the local weighted sum of pixels over the three colour channels of a given image (LeCun, Bengio,
124 and Hinton 2015). In practice, CNNs are fed with large amounts of images in which target objects
125 have been manually annotated so they can be trained to associate labels to a given object. During
126 this training phase, the weights are iteratively modified to obtain the desired answer by minimizing
127 the error function between the output of the CNN and the correct answer through a process called
128 backpropagation (LeCun, Bengio, and Hinton 2015). The final output of the CNN is a confidence
129 score for each of the learned objects.

130 We selected a Faster R-CNN network (Ren et al. 2016) publicly available from the Tensorflow
131 model zoo and tuned it for eagle ray detection on aerial images. The Faster R-CNN is a deep
132 learning algorithm specialized for object detection that consists of two fully-convolutional networks:
133 (1) a region proposal network, which predicts object positions along with their 'objectness' scores
134 and (2) a detection network, which extracts features from the proposed regions and provides class
135 labels for the bounding boxes. We specifically used a Faster-RCNN with a ResNet-101 backbone,
136 a deep architecture in which layers have been reformulated as residual functions of input layers,
137 leading to better optimization and increased accuracy. Our eagle ray detection framework followed
138 the three main steps detailed below: 1) Image pre-processing, 2) Model training and 3) Model
139 accuracy assessment. The eagle ray detection framework is illustrated in Figure 1.

140 **2.4. Image pre-processing**

141 A total of 314 ULM images containing at least one eagle ray (representing 372 individual
142 encounters) were extracted out of the 79,325 collected images (Table 1). Bounding boxes
143 surrounding eagle rays spanned on average 25 x 25 pixels (pi) on the 2,704 x 1,520 pi images,
144 corresponding to a ratio of 0.0002 between the bounding box area and the image area. To
145 maximize the detection of small eagle rays on ULM images, we split each image into four images
146 with half the original size (i.e., 1,352 x 760 pi). This yielded 308 images with eagle rays (353
147 individual encounters), as rays located across image boundaries were lost. Image splitting
148 approaches are known to efficiently boost detection accuracy by increasing the relative pixel area
149 of small objects with respect to the entire images, thereby limiting detail losses when images are
150 processed throughout the network (Unel, Ozkalayci, and Cigla 2019) .

151 Next, images were randomly partitioned, using 80% of images for the training (and validation)
152 subset (corresponding to approximately 250 images) and 20% of images (approx. 60 images) for
153 the testing subset. Full independence between subsets was ensured by selecting images
154 belonging to different videos between the subsets. The training subset was then artificially
155 augmented by applying random transformations to images, including rotations (by -10 to +10
156 degrees), translations (by -10 to +10 %), scaling (by 80 to 120%), horizontal and vertical flipping,
157 and contrast modification (i.e., multiplying all image pixels with a value ranging from 0.6 to 1.4).
158 Artificial data augmentation is a particularly efficient technique for improving the generalization
159 performance and accuracy of object detection models (Zoph et al., 2019).

160 **2.5 Model training**

161 We initialized our Faster R-CNN with pre-trained weights based on the COCO (Common Objects
162 in Context) dataset (Lin et al., 2015) downloaded from the Tensorflow model zoo. This process of
163 applying previously learned knowledge to solve a new problem, called transfer learning, improves

164 model accuracy and generalization when a limited annotated dataset is available (Chen, Zhang,
165 and Ouyang 2018). We then trained the Faster R-CNN using a stochastic gradient descent
166 optimizer with a momentum of 0.9 for the loss function (Qian, 1999). We applied a learning rate of
167 10^{-3} , a L2 regularization (with a lambda of 0.004), and a dropout of 50% to mitigate overfitting
168 (Srivastava et al., 2014). The training was stopped after 50,000 iterations to prevent overfitting as
169 indicated by an increasing loss function for the validation subset (Sarle, 1995).

170 **2.6 Model accuracy assessment**

171 The Faster R-CNN was then applied for eagle ray detection on the test subset and its accuracy
172 was evaluated using a 5-fold cross-validation. K-fold cross-validation is a common procedure for
173 evaluating machine learning models while preventing systematic biases due to the partitioning of
174 data subsets (Wong, 2015). The initialized model was trained five times, each time with a different
175 training subset and its accuracy was evaluated five times, each time on an independent test
176 subset.

177 We applied lenient thresholds of 50% for both the confidence score of predictions and the overlap
178 of predictions with observations, since minimizing false negatives is more crucial than avoiding
179 false positives in the case of rare megafauna species (Villon et al., 2020). As such, a predicted
180 bounding box that was associated with a confidence score of at least 50% and that overlapped at
181 least 50% in surface with an annotated eagle ray was considered a true positive (TP). Predicted
182 bounding boxes not corresponding to an annotated bounding box were false positives (FP), while
183 annotated bounding boxes not corresponding to a predicted bounding box were false negatives
184 (FN). For each cross-validation test subset, the number of TPs, FPs and FNs were computed and
185 performance metrics were calculated as described below.

186 Precision is the percentage of TPs with respect to all predictions (Equation (1)). It represents the
187 percentage of predictions that are correct (the closest to 1, the fewest false positives):

$$188 \text{ Precision} = \text{TP} / (\text{TP} + \text{FP}) \quad (1)$$

189 Recall (or sensitivity) is the percentage of TPs with respect to all annotated objects (Equation (2)).
190 It represents the percentage of positives that are actually predicted (the closest to 1, the fewest
191 false negatives):

$$192 \text{ Recall} = \text{TP} / (\text{TP} + \text{FN}) \quad (2)$$

193 Finally, the f1-score evaluates the balance between FPs and FNs. It is an overall measure of
194 accuracy calculated as the harmonic mean of precision and recall (Equation (3)).

$$195 \text{ F1-score} = 2 \times \text{Recall} \times \text{Precision} / (\text{Recall} + \text{Precision}) \quad (3)$$

196 Finally, the mean and standard deviation of the performance metrics were computed across the 5-
197 fold cross-validations splits.

198 We used the open-source Tensorflow object detection API version 1 (Abadi et al., 2016) in Python
199 version 3 for the training and testing of our model. One training process lasted on average 3 hours
200 on a NVIDIA Quadro P6000 GPU with 64 GB of RAM. The application of the model took on
201 average 5 seconds per image.

202 **2.7 Spatial distribution of eagle rays**

203 Locations of eagle ray occurrences obtained from both manual annotation and the deep learning
204 model were mapped in the study area by retrieving the GPS coordinates of their image identifiers.
205 Locations of all ULM tracks were also mapped by retrieving the GPS coordinates of all video
206 images. To account for the heterogeneous sampling effort, the encounter rate (individuals/km) was
207 mapped throughout the study area. To do so, we created a spatial grid of 0.005° longitude x 0.005°
208 latitude and summed the number of eagle rays and the length of ULM tracks in each cell. The
209 number of individuals was then divided by the length of ULM tracks per cell to obtain the encounter
210 rate. All maps were produced in R (version 4.0.3) with the OpenStreetMap (Fellows, 2019) and
211 ggplot2 packages (Wickham et al., 2020).

212 **3. Results**

213 **3.1 Deep learning model accuracy**

214 Our deep learning model trained with 255 images on average (range= 252 - 259 between cross-
215 validations) accurately detected eagle rays on independent images from the same lagoon. The
216 model reached a mean precision of 0.90 on test images (SD= 0.08), meaning that 90% of the
217 model predictions corresponded to a manually annotated eagle ray (i.e., were TPs) (Figure 2).
218 False positives were primarily associated with coral patches. The mean recall was 0.92 (SD=
219 0.06), meaning that 92% of the annotated eagle rays were detected (Figure 2). The model
220 successfully detected eagle rays in various contexts, as illustrated in Figure 2 and Supplementary
221 Figure D. The mean f1-score balancing FPs and FNs was 0.91 (SD= 0.06). Precision, recall and
222 the f1-score showed little sensitivity to the prediction confidence score (Figure 3).

223 **3.2 Spatial distribution of eagle rays**

224 Eagle rays detected from the deep learning model were distributed throughout the study area, but
225 appeared concentrated in a more intensively surveyed portion of the barrier reef near the
226 easternmost channel (Figure 4-a). The few FPs and FNs were scattered across the lagoon and on
227 the barrier reef (Supplementary Figure E-1). The encounter rate map, accounting for the

228 heterogeneous sampling effort, confirmed the slightly higher occurrence of eagle rays on the
229 barrier reef compared to the lagoon (Figure 4-b). The spatial distributions of detected eagle rays
230 and their encounter rates were similar to that of all annotated eagle rays (Supplementary Figures
231 E-2 and E-3).

232 **4. Discussion**

233 More than one third of all cartilaginous fishes are threatened with extinction, primarily due to
234 overfishing (Dulvy et al. 2021). Rays are no exception as they represent 56.3% of threatened
235 chondrichthyan and 12.3% of ray species are still lacking sufficient data for assessment (Dulvy et
236 al. 2021). As human activities continue to jeopardize these species (Pacoureaux et al., 2021; Yan et
237 al., 2021), there is an urgent need for reliable and efficient approaches for monitoring populations.
238 Our study revealed the potential of deep learning for the accurate detection of eagle rays in coral
239 reef ecosystems. Our model trained with fewer than 260 aerial images was able to detect 92% of
240 the eagle rays on independent images from the same lagoon. Our study paves the way towards
241 automated ray population monitoring in coral reefs by providing a fast and accurate alternative to
242 the manual processing of aerial images (Kelaher et al. 2020; Kiszka et al. 2016). While deep
243 learning for elasmobranch aerial detection has been applied in the context of beach surveillance
244 (Gorkin et al. 2020), we present its first implementation towards ecological and conservation
245 applications, including species distribution mapping).

246 **4.1. Eagle ray detection accuracy**

247 Our model achieved a very good detection performance despite the modest size of the training
248 dataset. Obtaining large amounts of images for training deep learning models is a major bottleneck
249 for ecological and conservation applications (Christin, Hervet, and Lecomte 2019). To overcome
250 this limitation, we relied on transfer learning and artificial data augmentation, two efficient
251 techniques that are widely used for training models in data-limited situations (Schneider et al.,
252 2020). The model was successful at avoiding missed occurrences (false negatives), which is most
253 critical when the objective is to detect vulnerable species that occur in low numbers such as rays
254 and sharks (Villon et al., 2020). Eagle rays were consistently detected across the diversity of
255 habitats (e.g., soft bottom and barrier reef) and acquisition conditions (e.g., luminosity, altitude and
256 camera angle) in our study area. The robustness of the model at detecting eagle rays in more
257 contexts and its generalization to new data could be further increased by expanding the size of
258 both the training and the test datasets and the contextual variety at new sites in New-Caledonia
259 and beyond. Moreover, there is a need to test the model's generalizability to a larger dataset in the
260 future, as the size of the test dataset is also limited. The model was equally successful at avoiding
261 false positives, with few misdetections primarily associated with coral patches. To eliminate these

262 false positives, coral patch annotations could be incorporated into the training dataset so that the
263 model explicitly learns this class. As deep learning algorithms rapidly improve, we could further
264 enhance our eagle ray detection method by using most up-to-date object detection CNNs such as
265 the YOLOv3 that achieved a high performance on fish detection (Jalal et al., 2020).

266 **4.2. Comparison with other monitoring methods**

267 Effective conservation requires up-to-date and high quality data collected with limited monetary
268 and human costs over repeated periods (Fust and Loos 2020). Previous studies on the distribution
269 and movements of eagle rays have relied on acoustic (DeGroot et al., 2020) and satellite telemetry
270 (Ajemian and Powers 2014). Active acoustic telemetry implies following the individuals in order to
271 determine their movements in the water column, but is generally restricted to few individuals and
272 necessitates a large array of hydrophones (DeGroot et al., 2020). Satellite telemetry allows
273 tracking rays over potentially large spatial scales, but is constrained by the frequency and precision
274 of GPS data and associated costs (Ajemian and Powers 2014). Both methods are intrusive as they
275 require catching and manipulating individuals to attach the tags properly. Surveys from scuba
276 divers and baited remote underwater videos (Rizzari, Frisch, and Magnenat 2014; Ward-Paige
277 2017) are also used for elasmobranch censuses, especially for species that live further from the
278 surface. However, these underwater surveys are limited in their spatial extent and may fail to
279 detect the most elusive species (Juhel et al., 2017). Moreover, observations may not be precisely
280 located and are not verifiable, unlike those derived from video footage.

281 In this study, aerial images collected from an off-the-shelf camera and processed with a deep
282 learning algorithm allowed us to precisely locate eagle rays in a coral lagoon at low financial and
283 operational costs. The opportunistic use of an aircraft dedicated to touristic flights led to an
284 heterogeneous survey effort, preventing the estimation of abundance from the traditional strip
285 transect methodology (Kiszka et al., 2016; Sykora-Bodie et al., 2017). Nevertheless, our accurate
286 algorithm will be applicable to images collected along systematically-designed transects for
287 abundance estimation in the future. Despite the heterogeneous survey effort, the current method
288 suggests a widespread distribution of eagle rays across a variety of coral reef habitats, which is in
289 accordance with previous study (Ajemian and Powers 2014). Future studies should seek to
290 quantify habitat preferences of eagle rays by linking effort-corrected encounter rates to local habitat
291 information (Ajemian, Powers, and Murdoch 2012; DeGroot et al. 2020).

292 Shark and ray monitoring requires detection and census methods that are adapted to the studied
293 habitats. While aerial surveys are very efficient in coral reefs with clear and shallow waters, open
294 water or turbid waters (e.g., estuaries, mangroves) require non-visual methods such as acoustic
295 telemetry. Environmental DNA is also an innovative method at the species level that can be
296 notably used to detect rare species including elasmobranchs (Boussarie et al., 2018). Coral

297 lagoons are major habitats for eagle rays (DeGroot et al. 2020; Ajemian, Powers, and Murdoch
298 2012) and our aerial approach proved efficient for monitoring populations in these habitats. Our
299 approach can be complemented by other methods (e.g., eDNA, acoustic telemetry) in habitats
300 where eagle rays can occur (Ajemian and Powers 2014; Sellas et al. 2015) but waters are deep or
301 turbid.

302 **4.3. Implications for elasmobranchs monitoring in coral reefs**

303 Data on population trends and distributions of rays and sharks are difficult to collect; yet, such
304 information is critical to establish appropriate conservation and management actions (Dwyer et al.,
305 2020; MacNeil et al., 2020; Pacoureau et al., 2021). Our approach combining video-surveys and
306 deep learning offers a potential breakthrough for the automated monitoring of eagle rays in coral
307 reef ecosystems. The ability of our model at detecting eagle rays in the variety of habitats and
308 conditions encompassed by our data highlights its potential robustness in a broad range of
309 contexts. Future work should assess the model transferability to other coral lagoons in New
310 Caledonia and beyond. Robust detection models would be particularly beneficial for ray monitoring
311 in the Indo-Pacific biodiversity triangle where conservation efforts are most urgent due to
312 pronounced levels of human threats (Dulvy et al. 2021). Our deep learning approach could be
313 applied to other distinctive elasmobranchs, provided sufficient images of these species are
314 available for training the model.

315 Finally, our approach could be extended to systematic video-surveys from manned aircraft or
316 drones to not only detect individuals, but also count them to derive abundance estimates and
317 species density maps in a study area. Drones make a viable alternative to manned aircraft for
318 marine megafauna surveys (Gray et al., 2018; Hodgson et al., 2013; Kelaher et al., 2020; Kiszka et
319 al., 2016), alleviating safety risks, monetary costs and carbon emissions (Hodgson et al., 2013).
320 However, the use of drones is subject to strict airspace regulations, and legislation in many areas
321 necessitates the pilot to maintain visual-line-of-sight with the drone (Raoult et al., 2020). The
322 platform choice will ultimately depend on the study question and the required imagery
323 characteristics. Using an aircraft dedicated to touristic flights allowed us to achieve greater spatial
324 and temporal coverage than would have been possible with a single drone and with no need to
325 acquire permits. This method could be implemented in other touristic locations (e.g., Australia,
326 French Polynesia, the Caribbean) where local companies operate scenic, low altitude flights over
327 coastal areas.

328 Overall, our cost-effective approach succeeded in collecting high-quality images for training a deep
329 learning model able to detect 92% of eagle rays in coral reefs. This new eagle ray detector will be
330 critical for deriving abundance estimates in order to closely monitor these vulnerable populations in
331 the future.

332 **Author contributions**

333 LM, DM, LV and MC conceived the ideas and designed the methodology; LM, LV and DM
334 collected the data; LM and LD analysed the data and developed scripts; LD and LM led the writing
335 of the manuscript. All authors contributed critically to the drafts and gave final approval for
336 publication.

337 **Data statement**

338 The eagle ray image database will be made available on Zenodo.

339 **References**

- 340 Abadi, M., Agarwal, A., Barham, P., Brevdo, E., Chen, Z., Citro, C., Corrado, G. S., Davis, A.,
341 Dean, J., Devin, M., Ghemawat, S., Goodfellow, I., Harp, A., Irving, G., Isard, M., Jia, Y.,
342 Jozefowicz, R., Kaiser, L., Kudlur, M., ... Zheng, X. (2016). TensorFlow : Large-Scale
343 Machine Learning on Heterogeneous Distributed Systems. *ArXiv:1603.04467 [Cs]*.
344 <http://arxiv.org/abs/1603.04467>
- 345 Ajemian, M. J., & Powers, S. P. (2014). Towed-float satellite telemetry tracks large-scale
346 movement and habitat connectivity of myliobatid stingrays. *Environ Biol Fish*, 15.
- 347 Ajemian, M. J., Powers, S. P., & Murdoch, T. J. T. (2012). Estimating the Potential Impacts of
348 Large Mesopredators on Benthic Resources : Integrative Assessment of Spotted Eagle Ray
349 Foraging Ecology in Bermuda. *PLoS ONE*, 7(7), e40227.
350 <https://doi.org/10.1371/journal.pone.0040227>
- 351 Boussarie, G., Bakker, J., Wangensteen, O. S., Mariani, S., Bonnin, L., Juhel, J.-B., Kiszka, J. J.,
352 Kulbicki, M., Manel, S., Robbins, W. D., Vigliola, L., & Mouillot, D. (2018). Environmental
353 DNA illuminates the dark diversity of sharks. *Science Advances*, 4(5), eaap9661.
354 <https://doi.org/10.1126/sciadv.aap9661>
- 355 Ceccarelli, D. M., McKinnon, A. D., Andréfouët, S., Allain, V., Young, J., Gledhill, D. C., Flynn, A.,
356 Bax, N. J., Beaman, R., Borsa, P., Brinkman, R., Bustamante, R. H., Campbell, R., Cappel,
357 M., Cravatte, S., D'Agata, S., Dichmont, C. M., Dunstan, P. K., Dupouy, C., ... Richardson,

358 A. J. (2013). The Coral Sea. In *Advances in Marine Biology* (Vol. 66, p. 213- 290). Elsevier.
359 <https://doi.org/10.1016/B978-0-12-408096-6.00004-3>

360 Chen, Z., Zhang, T., & Ouyang, C. (2018). End-to-End Airplane Detection Using Transfer Learning
361 in Remote Sensing Images. *Remote Sensing*, 10(1), 139.
362 <https://doi.org/10.3390/rs10010139>

363 Christin, S., Hervet, É., & Lecomte, N. (2019). Applications for deep learning in ecology. *Methods*
364 *in Ecology and Evolution*, 10(10), 1632- 1644. <https://doi.org/10.1111/2041-210X.13256>

365 Colefax, A. P., Butcher, P. A., & Kelaher, B. P. (2018). The potential for unmanned aerial vehicles
366 (UAVs) to conduct marine fauna surveys in place of manned aircraft. *ICES Journal of*
367 *Marine Science*, 75(1), 1- 8. <https://doi.org/10.1093/icesjms/fsx100>

368 DeGroot, B., Roskar, G., Brewster, L., & Ajemian, M. (2020). Fine-scale movement and habitat use
369 of whitespotted eagle rays *Aetobatus narinari* in the Indian River Lagoon, Florida, USA.
370 *Endangered Species Research*, 42, 109- 124. <https://doi.org/10.3354/esr01047>

371 Ditria, E. M. (2020). Automating the Analysis of Fish Abundance Using Object Detection :
372 Optimizing Animal Ecology With Deep Learning. *Frontiers in Marine Science*, 7, 9.

373 Dujon, A. M., Ierodiaconou, D., Geeson, J. J., Arnould, J. P. Y., Allan, B. M., Katselidis, K. A., &
374 Schofield, G. (2021). Machine learning to detect marine animals in UAV imagery : Effect of
375 morphology, spacing, behaviour and habitat. *Remote Sensing in Ecology and*
376 *Conservation*, 7(3), 341- 354. <https://doi.org/10.1002/rse2.205>

377 Dulvy, N. K., Carlson, J., Charvet, P., Ajemian, M. J., Bassos-Hull, K., Blanco-Parra, M., Chartrain,
378 E., Derrick, D., Dia, M., Diop, M., Doherty, P., Dossa, J., De Bruyne, G., Herman, K., Leurs,
379 G. H. L., Mejía-Falla, P. A., Navia, A. F., Pacoureau, N., Pérez Jiménez, J. C., ... Williams,
380 A. B. (2020). *Aetobatus narinari* : *The IUCN Red List of Threatened Species 2021* [Data
381 set]. International Union for Conservation of Nature. [https://doi.org/10.2305/IUCN.UK.2021-](https://doi.org/10.2305/IUCN.UK.2021-2.RLTS.T42564343A201613657.en)
382 [2.RLTS.T42564343A201613657.en](https://doi.org/10.2305/IUCN.UK.2021-2.RLTS.T42564343A201613657.en)

383 Dulvy, N. K., Pacoureau, N., Rigby, C. L., Pollom, R. A., Jabado, R. W., Ebert, D. A., Finucci, B.,
384 Pollock, C. M., Cheok, J., Derrick, D. H., Herman, K. B., Sherman, C. S., VanderWright, W.
385 J., Lawson, J. M., Walls, R. H. L., Carlson, J. K., Charvet, P., Bineesh, K. K., Fernando, D.,

386 ... Simpfendorfer, C. A. (2021). Overfishing drives over one-third of all sharks and rays
387 toward a global extinction crisis. *Current Biology*, 31(21), 4773-4787.e8.
388 <https://doi.org/10.1016/j.cub.2021.08.062>

389 Dwyer, R. G., Krueck, N. C., Udyawer, V., Heupel, M. R., Chapman, D., Pratt, H. L., Garla, R., &
390 Simpfendorfer, C. A. (2020). Individual and Population Benefits of Marine Reserves for
391 Reef Sharks. *Current Biology*, 30(3), 480-489.e5. <https://doi.org/10.1016/j.cub.2019.12.005>

392 Eikelboom, J. A. J., Wind, J., van de Ven, E., Kenana, L. M., Schroder, B., de Knecht, H. J.,
393 van Langevelde, F., & Prins, H. H. T. (2019). Improving the precision and accuracy of
394 animal population estimates with aerial image object detection. *Methods in Ecology and*
395 *Evolution*, 10(11), 1875- 1887. <https://doi.org/10.1111/2041-210X.13277>

396 Fellows, I. (2019). *OpenStreetMap : Access to Open Street Map Raster Images*. [https://CRAN.R-](https://CRAN.R-project.org/package=OpenStreetMap)
397 [project.org/package=OpenStreetMap](https://CRAN.R-project.org/package=OpenStreetMap)

398 Fricke, R., Kulbicki, M., & Wantiez, L. (2011). Checklist of the fishes of New Caledonia, and their
399 distribution in the Southwest Pacific Ocean (Pisces). *STUTTGARTER BEITRÄGE ZUR*
400 *NATURKUNDE A*, 123.

401 Froese, R., & Pauly, D. (2021). Froese, R. and D. Pauly. Editors. 2021.FishBase. World Wide Web
402 electronic publication. www.fishbase.org, (06/2021). *FishBase. World Wide Web*
403 *electronic publication. www.fishbase.org, (06/2021).*

404 Fust, P., & Loos, J. (2020). Development perspectives for the application of autonomous,
405 unmanned aerial systems (UASs) in wildlife conservation. *Biological Conservation*, 241,
406 108380. <https://doi.org/10.1016/j.biocon.2019.108380>

407 Gorkin, R., Adams, K., Berryman, M. J., Aubin, S., Li, W., Davis, A. R., & Barthelemy, J. (2020).
408 Sharkeye : Real-Time Autonomous Personal Shark Alerting via Aerial Surveillance. *Drones*,
409 4(2), 18. <https://doi.org/10.3390/drones4020018>

410 Gray, P. C., Bierlich, K. C., Mantell, S. A., Friedlaender, A. S., Goldbogen, J. A., & Johnston, D. W.
411 (2019). Drones and convolutional neural networks facilitate automated and accurate
412 cetacean species identification and photogrammetry. *Methods in Ecology and Evolution*,
413 10(9), 1490- 1500. <https://doi.org/10.1111/2041-210X.13246>

414 Gray, P. C., Fleishman, A. B., Klein, D. J., McKown, M. W., Bézy, V. S., Lohmann, K. J., &
415 Johnston, D. W. (2018). A Convolutional Neural Network for Detecting Sea Turtles in Drone
416 Imagery. *Methods in Ecology and Evolution*, 2041-210X.13132.
417 <https://doi.org/10.1111/2041-210X.13132>

418 Guirado, E., Tabik, S., Rivas, M. L., Alcaraz-Segura, D., & Herrera, F. (2019). Whale counting in
419 satellite and aerial images with deep learning. *Scientific Reports*, 9(1), 14259.
420 <https://doi.org/10.1038/s41598-019-50795-9>

421 Hodgson, A., Kelly, N., & Peel, D. (2013). Unmanned Aerial Vehicles (UAVs) for Surveying Marine
422 Fauna : A Dugong Case Study. *PLOS ONE*, 8(11), e79556.
423 <https://doi.org/10.1371/journal.pone.0079556>

424 Jabado, R. W., Kyne, P. M., Pollom, R. A., Ebert, D. A., Simpfendorfer, C. A., Ralph, G. M.,
425 Dhaheri, S. S. A., Akhilesh, K. V., Ali, K., Ali, M. H., Mamari, T. M. S. A., Bineesh, K. K.,
426 Hassan, I. S. E., Fernando, D., Grandcourt, E. M., Khan, M. M., Moore, A. B. M., Owfi, F.,
427 Robinson, D. P., ... Dulvy, N. K. (2018). Troubled waters : Threats and extinction risk of the
428 sharks, rays and chimaeras of the Arabian Sea and adjacent waters. *Fish and Fisheries*,
429 19(6), 1043- 1062. <https://doi.org/10.1111/faf.12311>

430 Jalal, A., Salman, A., Mian, A., Shortis, M., & Shafait, F. (2020). Fish detection and species
431 classification in underwater environments using deep learning with temporal information.
432 *Ecological Informatics*, 57, 101088. <https://doi.org/10.1016/j.ecoinf.2020.101088>

433 Juhel, J.-B., Vigliola, L., Mouillot, D., Kulbicki, M., Letessier, T. B., Meeuwig, J. J., & Wantiez, L.
434 (2017). *Reef accessibility impairs the protection of sharks*. 11.

435 Kelaher, B. P., Colefax, A. P., Tagliafico, A., Bishop, M. J., Giles, A., & Butcher, P. A. (2020).
436 Assessing variation in assemblages of large marine fauna off ocean beaches using drones.
437 *Marine and Freshwater Research*, 71(1), 68. <https://doi.org/10.1071/MF18375>

438 Kelaher, B., Peddemors, V., Hoade, B., Colefax, A., & Butcher, P. (2019). Comparison of sampling
439 precision for nearshore marine wildlife using unmanned and manned aerial surveys.
440 *Journal of Unmanned Vehicle Systems*, 32.

441 Kiszka, J., Mourier, J., Gastrich, K., & Heithaus, M. (2016). Using unmanned aerial vehicles

442 (UAVs) to investigate shark and ray densities in a shallow coral lagoon. *Marine Ecology*
443 *Progress Series*, 560, 237- 242. <https://doi.org/10.3354/meps11945>

444 Last, P. R., White, W. T., & Pogonoski, J. J. (2010). *Descriptions of new sharks and rays from*
445 *Borneo*. CSIRO Marine & Atmospheric Research.

446 LeCun, Y., Bengio, Y., & Hinton, G. (2015a). Deep learning. *Nature*, 521(7553), 436- 444.
447 <https://doi.org/10.1038/nature14539>

448 LeCun, Y., Bengio, Y., & Hinton, G. (2015b). Deep learning. *Nature*, 521(7553), 436- 444.
449 <https://doi.org/10.1038/nature14539>

450 Lin, T.-Y., Maire, M., Belongie, S., Bourdev, L., Girshick, R., Hays, J., Perona, P., Ramanan, D.,
451 Zitnick, C. L., & Dollár, P. (2015). Microsoft COCO : Common Objects in Context.
452 *ArXiv:1405.0312 [Cs]*. <http://arxiv.org/abs/1405.0312>

453 MacNeil, M. A., Chapman, D. D., Heupel, M., Simpfendorfer, C. A., Heithaus, M., Meekan, M.,
454 Harvey, E., Goetze, J., Kiszka, J., Bond, M. E., Currey-Randall, L. M., Speed, C. W.,
455 Sherman, C. S., Rees, M. J., Udyawer, V., Flowers, K. I., Clementi, G., Valentin-Albanese,
456 J., Gorham, T., ... Cinner, J. E. (2020). Global status and conservation potential of reef
457 sharks. *Nature*, 583(7818), 801- 806. <https://doi.org/10.1038/s41586-020-2519-y>

458 Mannocci, L., Villon, S., Chaumont, M., Guellati, N., Mouquet, N., Iovan, C., Vigliola, L., & Mouillot,
459 D. (2021). Leveraging social media and deep learning to detect rare megafauna in video
460 surveys. *Conservation Biology*, *cobi.13798*. <https://doi.org/10.1111/cobi.13798>

461 Norouzzadeh, M. S., Nguyen, A., Kosmala, M., Swanson, A., Palmer, M. S., Packer, C., & Clune,
462 J. (2018). Automatically identifying, counting, and describing wild animals in camera-trap
463 images with deep learning. *Proceedings of the National Academy of Sciences*, 115(25),
464 E5716- E5725. <https://doi.org/10.1073/pnas.1719367115>

465 Pacoureau, N., Rigby, C. L., Kyne, P. M., Sherley, R. B., Winker, H., Carlson, J. K., Fordham, S.
466 V., Barreto, R., Fernando, D., Francis, M. P., Jabado, R. W., Herman, K. B., Liu, K.-M.,
467 Marshall, A. D., Pollom, R. A., Romanov, E. V., Simpfendorfer, C. A., Yin, J. S., Kindsvater,
468 H. K., & Dulvy, N. K. (2021). Half a century of global decline in oceanic sharks and rays.
469 *Nature*, 589(7843), 567- 571. <https://doi.org/10.1038/s41586-020-03173-9>

470 Padubidri, C., Kamilaris, A., Karatsiolis, S., & Kamminga, J. (2021). Counting sea lions and
471 elephants from aerial photography using deep learning with density maps. *Animal*
472 *Biotelemetry*, 9(1), 27. <https://doi.org/10.1186/s40317-021-00247-x>

473 Qian, N. (1999). On the momentum term in gradient descent learning algorithms. *Neural Networks*,
474 12(1), 145- 151. [https://doi.org/10.1016/S0893-6080\(98\)00116-6](https://doi.org/10.1016/S0893-6080(98)00116-6)

475 Raoult, V., Colefax, A. P., Allan, B. M., Cagnazzi, D., Castelblanco-Martínez, N., Ierodiaconou, D.,
476 Johnston, D. W., Landeo-Yauri, S., Lyons, M., Pirotta, V., Schofield, G., & Butcher, P. A.
477 (2020). Operational Protocols for the Use of Drones in Marine Animal Research. *Drones*,
478 4(4), 64. <https://doi.org/10.3390/drones4040064>

479 Ren, S., He, K., Girshick, R., & Sun, J. (2016). Faster R-CNN : Towards Real-Time Object
480 Detection with Region Proposal Networks. *ArXiv:1506.01497 [Cs]*.
481 <http://arxiv.org/abs/1506.01497>

482 Rieucan, G., Kiszka, J. J., Castillo, J. C., Mourier, J., Boswell, K. M., & Heithaus, M. R. (2018).
483 Using unmanned aerial vehicle (UAV) surveys and image analysis in the study of large
484 surface-associated marine species : A case study on reef sharks *Carcharhinus*
485 *melanopterus* shoaling behaviour. *Journal of Fish Biology*, 93(1), 119- 127.
486 <https://doi.org/10.1111/jfb.13645>

487 Rigby, C. L., Bin Ali, A., Chen, X., Derrick, C., Dharmadi Ebert, D. A., Fahmi Fernando, D.,
488 Gautama, D. A., Haque, A. B., Herman, K., Ho, H., Hsu, H., Krajangdara, T., Maung, A.,
489 Seyha, L., Sianipar, A., Tanay, D., Utzurrum, J.-A. T., Vo, V. Q., Yuneni, R. R., & Zhang, J.
490 (2020). *Aetomylaeus maculatus* : *The IUCN Red List of Threatened Species 2020*.
491 International Union for Conservation of Nature.
492 <https://www.iucnredlist.org/species/60120/124440727>

493 Rizzari, J. R., Frisch, A. J., & Magnenat, K. A. (2014). Diversity, abundance, and distribution of reef
494 sharks on outer-shelf reefs of the Great Barrier Reef, Australia. *Marine Biology*, 161(12),
495 2847- 2855. <https://doi.org/10.1007/s00227-014-2550-3>

496 Sarle, W. S. (1995). *Stopped training and other remedies for overfitting*. Computer Science.

497 Schneider, S., Greenberg, S., Taylor, G. W., & Kremer, S. C. (2020). Three critical factors affecting

498 automated image species recognition performance for camera traps. *Ecology and*
499 *Evolution*, 10(7), 3503- 3517. <https://doi.org/10.1002/ece3.6147>

500 Schofield, G., Papafitsoros, K., Haughey, R., & Katselidis, K. (2017). Aerial and underwater
501 surveys reveal temporal variation in cleaning-station use by sea turtles at a temperate
502 breeding area. *Marine Ecology Progress Series*, 575, 153- 164.
503 <https://doi.org/10.3354/meps12193>

504 Sellas, A. B., Bassos-Hull, K., Perez-Jimenez, J. C., Angulo-Valdes, J. A., Bernal, M. A., & Hueter,
505 R. E. (2015). Population Structure and Seasonal Migration of the Spotted Eagle Ray,
506 *Aetobatus narinari*. *Journal of Heredity*, 106(3), 266- 275.
507 <https://doi.org/10.1093/jhered/esv011>

508 Srivastava, N., Hinton, G., Krizhevsky, A., Sutskever, I., & Salakhutdinov, R. (2014). Dropout : A
509 Simple Way to Prevent Neural Networks from Overfitting. *Journal of Machine Learning*
510 *Research*, 30.

511 Sykora-Bodie, S. T., Bezy, V., Johnston, D. W., Newton, E., & Lohmann, K. J. (2017). Quantifying
512 Nearshore Sea Turtle Densities : Applications of Unmanned Aerial Systems for Population
513 Assessments. *Scientific Reports*, 7(1), 17690. <https://doi.org/10.1038/s41598-017-17719-x>

514 Torney, C. J., Lloyd- Jones, D. J., Chevallier, M., Moyer, D. C., Maliti, H. T., Mwita, M., Kohi, E. M.,
515 & Hopcraft, G. C. (2019). A comparison of deep learning and citizen science techniques for
516 counting wildlife in aerial survey images. *Methods in Ecology and Evolution*, 10(6),
517 779- 787. <https://doi.org/10.1111/2041-210X.13165>

518 Unel, F. O., Ozkalayci, B. O., & Cigla, C. (2019). The Power of Tiling for Small Object Detection.
519 *2019 IEEE/CVF Conference on Computer Vision and Pattern Recognition Workshops*
520 *(CVPRW)*, 582- 591. <https://doi.org/10.1109/CVPRW.2019.00084>

521 Villon, S., Mouillot, D., Chaumont, M., Darling, E. S., Subsol, G., Claverie, T., & Villéger, S. (2018).
522 A Deep learning method for accurate and fast identification of coral reef fishes in
523 underwater images. *Ecological Informatics*, 48, 238- 244.
524 <https://doi.org/10.1016/j.ecoinf.2018.09.007>

525 Villon, S., Mouillot, D., Chaumont, M., Subsol, G., Claverie, T., & Villéger, S. (2020). A new method

526 to control error rates in automated species identification with deep learning algorithms.
527 *Scientific Reports*, 10(1), 10972. <https://doi.org/10.1038/s41598-020-67573-7>

528 Ward-Paige, C. A. (2017). Global evaluation of shark sanctuaries. *Global Environmental Change*,
529 16.

530 Wickham, H., Chang, W., Henry, L., Pedersen, T. L., Takahashi, K., Wilke, C., Woo, K., Yutani, H.,
531 & Dewey, D. (2020). *ggplot2: Create Elegant Data Visualisations Using the Grammar of*
532 *Graphics*. <https://cran.r-project.org/web/packages/ggplot2/index.html>

533 Wong, T.-T. (2015). Performance evaluation of classification algorithms by k-fold and leave-one-
534 out cross validation. *Pattern Recognition*, 48(9), 2839- 2846.
535 <https://doi.org/10.1016/j.patcog.2015.03.009>

536 Yan, H. F., Kyne, P. M., Jabado, R. W., Leeney, R. H., Davidson, L. N. K., Derrick, D. H., Finucci,
537 B., Freckleton, R. P., Fordham, S. V., & Dulvy, N. K. (2021). Overfishing and habitat loss
538 drive range contraction of iconic marine fishes to near extinction. *Science Advances*, 7(7),
539 eabb6026. <https://doi.org/10.1126/sciadv.abb6026>

540 Zoph, B., Cubuk, E. D., Ghiasi, G., Lin, T.-Y., Shlens, J., & Le, Q. V. (2019). Learning Data
541 Augmentation Strategies for Object Detection. *ArXiv:1906.11172 [Cs]*.
542 <http://arxiv.org/abs/1906.11172>

543

544 **Tables**

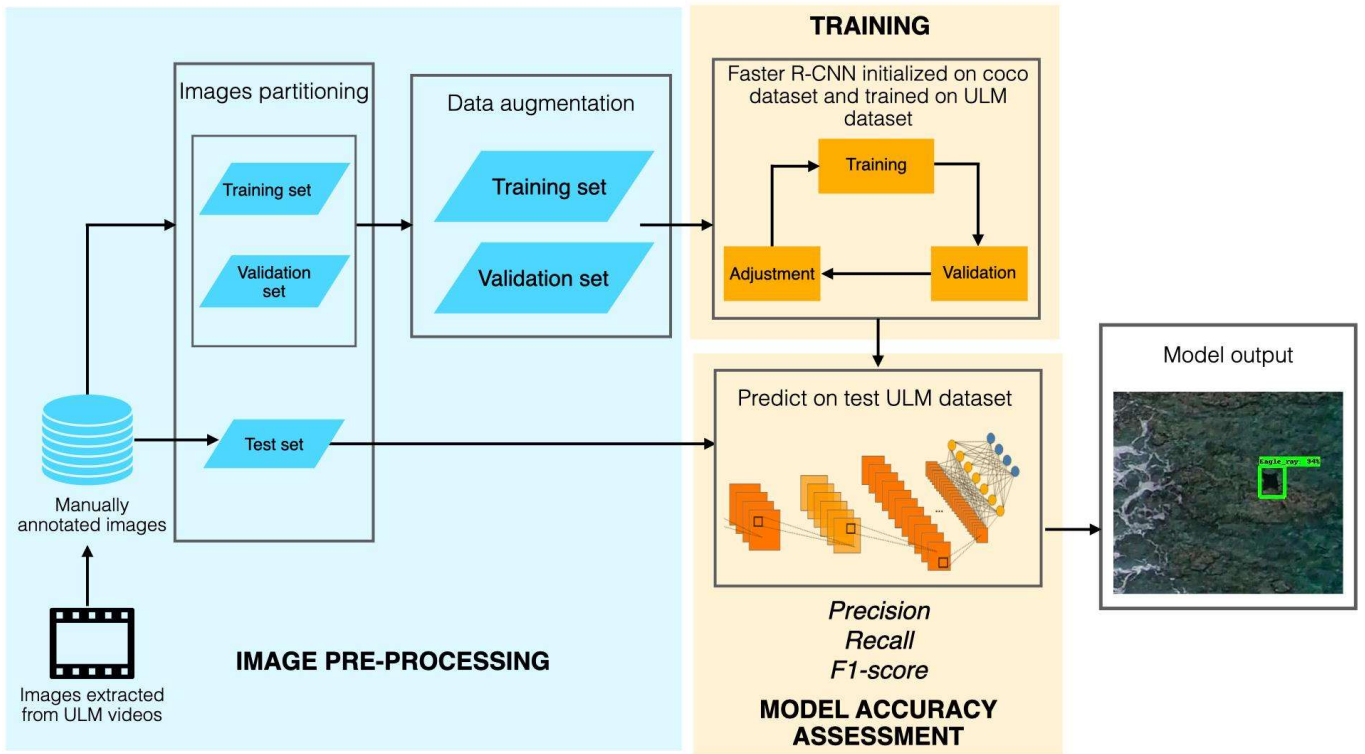
545 **Table 1:** Overview of the New Caledonia video database. Abbreviations: SD= standard deviation,
 546 pi= pixels.

Number of videos	Mean video duration	Total video duration	Total number of images	Number of images with ≥ 1 eagle ray		Number of individual encounters	
				2,704 x 1,520 pi images	1,352 x 760 pi images	2,704 x 1,520 pi images	1,352 x 760 pi images
114	11.70 min (SD= 0.93 min) equivalent to 11 min 42 s	22 h 14 min 19 s	79,325	314	308	372	353

547

548

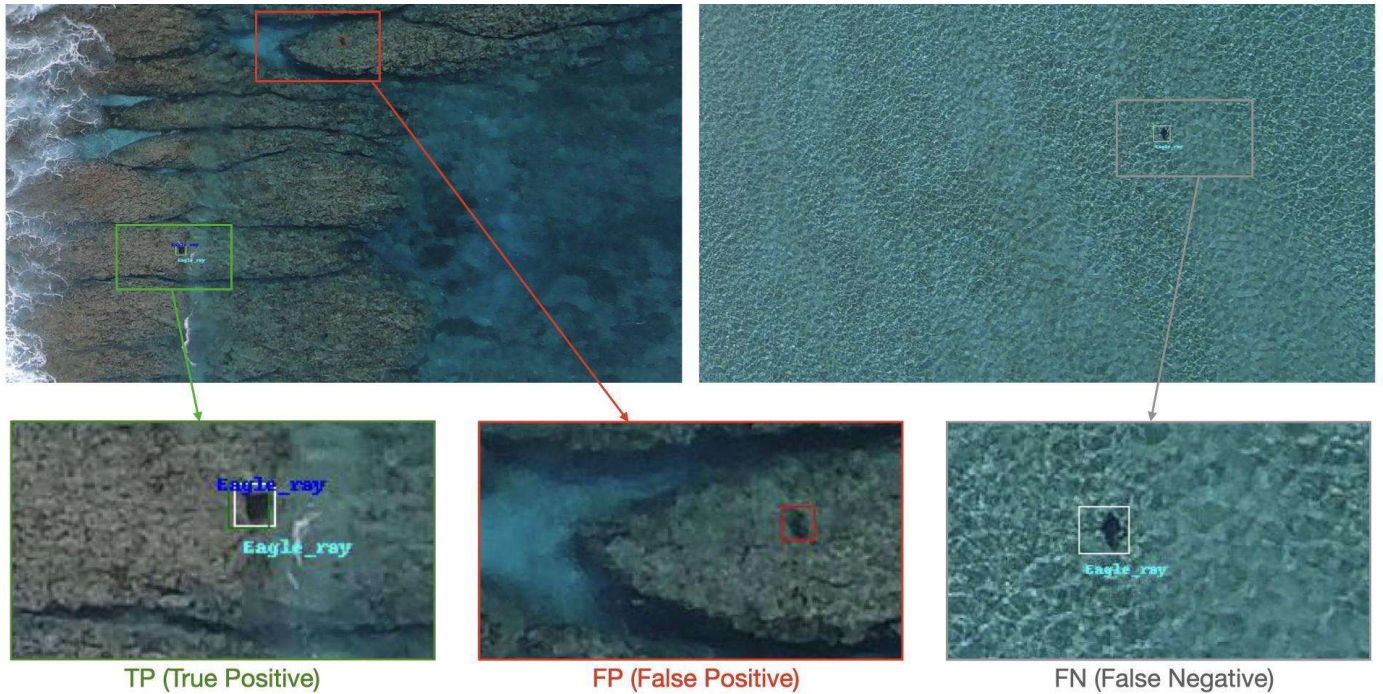
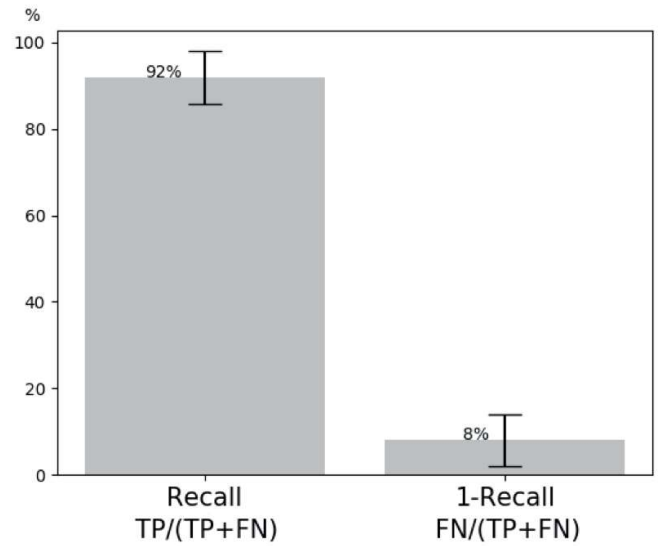
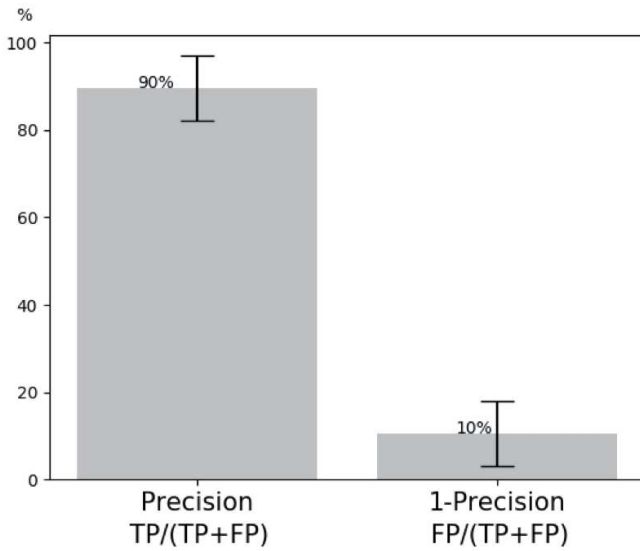
549



551
 552 **Figure 1:** Eagle ray detection framework with three main steps. 1) Image pre-processing: Images
 553 are extracted from the ULM videos and manually annotated. These images are then partitioned
 554 into independent training, validation and test sets. Training and validation sets are augmented by
 555 applying random transformations such as rotations and translations to images. 2) Training: A
 556 Faster R-CNN with weights pre-trained on the COCO dataset is downloaded from the Tensorflow
 557 model zoo and trained on the training set. The training is stopped before overfitting as indicated by
 558 an increasing loss function for the validation set. 3) Model accuracy assessment: The trained
 559 Faster R-CNN is applied for eagle ray detection on the test set. Precision, recall and the f1-score
 560 are then derived to evaluate the model accuracy. The final output is a detected bounding box with
 561 an associated confidence score for each of the detected eagle rays. These steps are detailed in
 562 sections 2.4., 2.5. and 2.6.

563
 564
 565
 566
 567

568



569

570

571

572

573

574

575

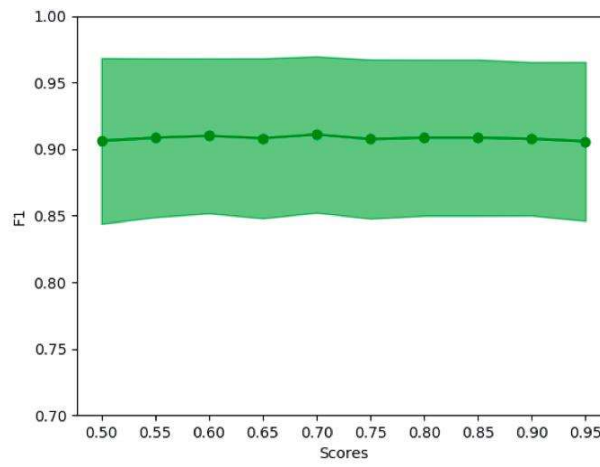
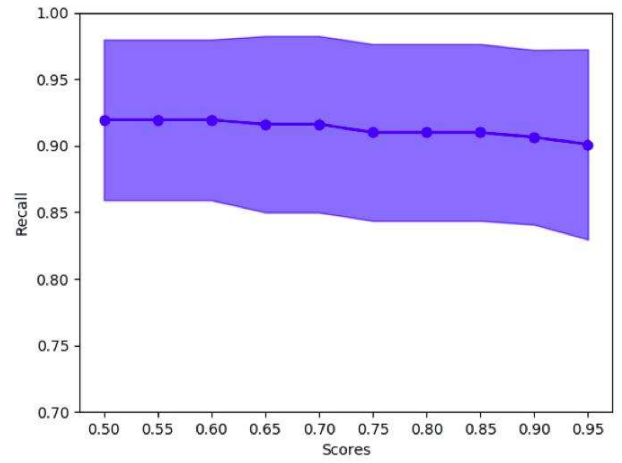
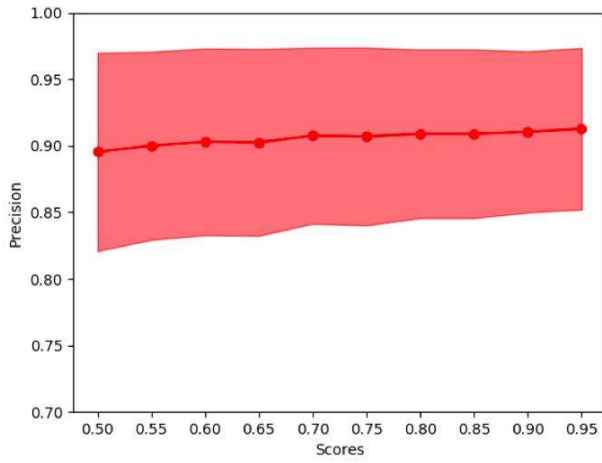
576

577

578

579

Figure 2: Results of eagle ray detection on test images for a prediction confidence score of 50%. The left graph shows the mean percentage of true positives (TPs) and false positives (FPs) with respect to all predictions. The right graph shows the mean percentage of TPs and false negatives (FNs) in the observations. The error bars are the standard deviations from the means. Examples are provided below the graphs for a TP in green (prediction associated with an annotation shown in white), a FP in red (prediction not corresponding to an annotation; here a coral patch) and a FN (annotation not corresponding to a prediction). Further examples of detection results are provided in Appendix D.

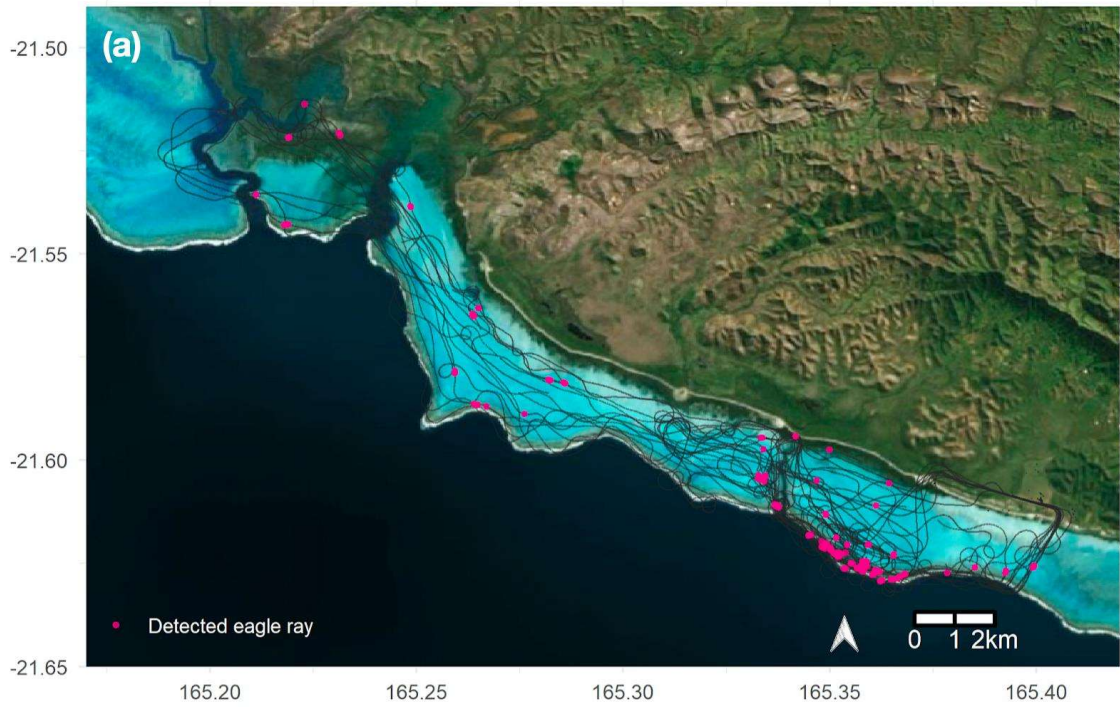


580

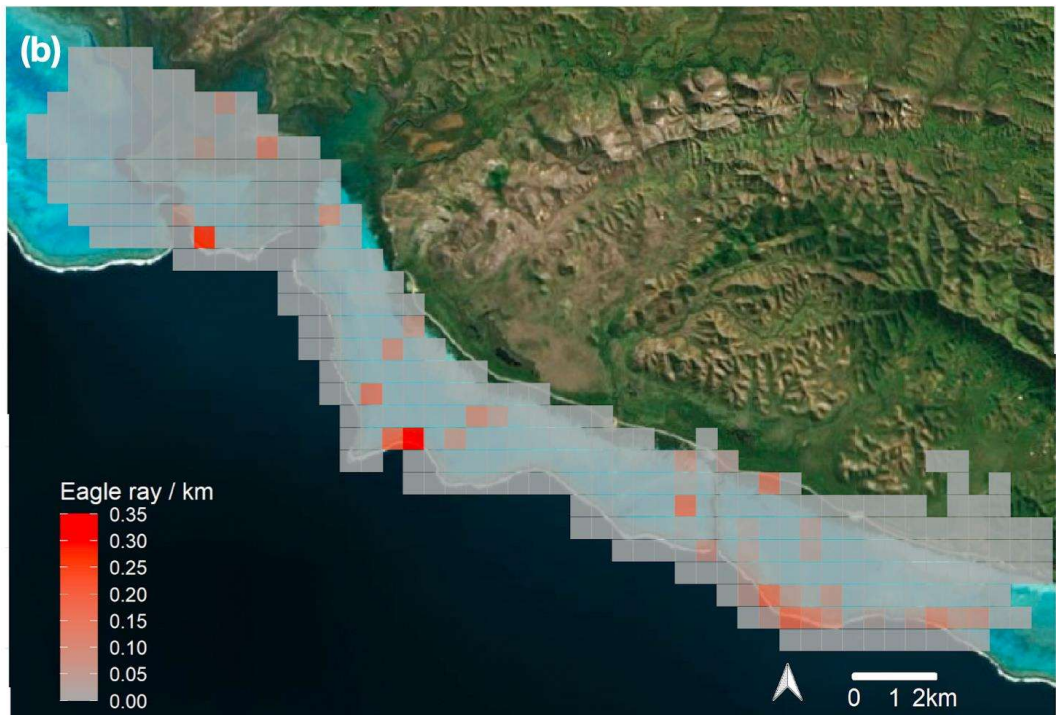
581 **Figure 3:** Mean precision, recall and f1-score on the test images for varying prediction confidence
 582 scores. The standard deviation is represented by the shaded area.

583

584



585



586

587 **Figure 4:** Spatial distribution of (a) eagle ray detections (dots) from the deep learning model
 588 mapped by retrieving the GPS coordinates of their image identifiers and the corresponding ULM
 589 flight tracks (black lines) and (b) the encounter rate (individuals/km) of detected eagle rays
 590 calculated on a spatial grid of 0.005° longitude x 0.005° latitude (the calculation is detailed in
 591 section 2.7).

Putting eagle rays on the map by coupling aerial video-surveys and deep learning

Authors: Desgarnier L.¹, Mouillot D.^{1,2}, Vigliola L.³, Chaumont M.^{4,5}, Mannocci L.^{1,3,4}

¹ MARBEC (Univ Montpellier, CNRS, Ifremer, IRD), Montpellier, France.

² Institut Universitaire de France, Paris, France.

³ ENTROPIE (IRD, Université de la Réunion, Université de la Nouvelle Calédonie, CNRS, Ifremer), Noumea, New Caledonia, France.

⁴ LIRMM (Université de Montpellier, CNRS), Montpellier, France.

⁵ Université de Nîmes, Nîmes, France.

Corresponding author: Lila Desgarnier

liladesgarnier@gmail.com

MARBEC Laboratory, 93 Place Eugène Bataillon, 34090 Montpellier, France

Acknowledgements

We are grateful to Jugurtha Ifticen, Lola Romant, Nacim Guellati, Gwendal Quimbre and Matis Toitot for their help with visualisation of ULM videos and annotation of images. We thank Air Paradise for their collaboration in collecting ULM video sequences in New Caledonia. This project received funding from the European Union's Horizon 2020 research and innovation programme under the Marie Skłodowska-Curie grant agreement No 845178 ('MEGAFAUNA').